Naval Surface Warfare Center
Carderock Division
West Bethesda, MD 20817-5700

CRDKNSWC/HD-1362-06 July 1998

Hydromechanics Directorate

Research and Development Report

Force and Moment Calculations of an Appendage Using the Reynolds Averaged Navier-Stokes Equations

By

Joseph J. Gorski

Gregory M. Buley

CRDKNSWC/HD-1362-06 Force and Moment Calculations of an Appendage Using the Reynolds Averaged Navier-Stokes Equations

REPORT DOCUMENTATION PAGE

Form Approved
OMB No. 0704-0188

1. AGENCY USE ONLY *(Leave blank)*	2. REPORT DATE	3. REPORT TYPE AND DATES COVERED
	July 1998	R & D Final

4. TITLE AND SUBTITLE
Force and Moment Calculations of an Appendage Using the Reynolds Averaged Navier-Stokes Equations

5. FUNDING NUMBERS

6. AUTHOR(S)
Joseph J. Gorski & Gregory M. Buley

7. PERFORMING ORGANIZATION NAME(S) AND ADDRESS(ES)
Naval Surface Warfare Center
Carderock Division
9500 MacArthur Boulevard
West Bethesda, MD 20817-5700

8. PERFORMING ORGANIZATION REPORT NUMBER
CRDKNSWC/HD-1362-06

9. SPONSORING/MONITORING AGENCY NAME(S) AND ADDRESS(ES)

10. SPONSORING/MONITORING AGENCY REPORT NUMBER

11. SUPPLEMENTARY NOTES

12a. DISTRIBUTION/AVAILABILITY STATEMENT
Approved for public release; distribution is unlimited.

12b. DISTRIBUTION CODE

13. ABSTRACT ***(Maximum 200 words)***

This report describes efforts to compute forces and moments about an appendage using the Reynolds averaged Navier-Stokes (RANS) equations. All computations presented are done with the Mississippi State University code UNCLE. Calculations are performed for a two-dimensional NACA 0012 airfoil and a three-dimensional NACA 0015 low-aspect ratio appendage mounted on a ground board. Results are presented for both forward and reverse flow conditions.

14. SUBJECT TERMS
Navier-Stokes equations appendages

15. NUMBER OF PAGES
28

16. PRICE CODE

17. SECURITY CLASSIFICATION OF REPORT	18. SECURITY CLASSIFICATION OF THIS PAGE	19. SECURITY CLASSIFICATION OF ABSTRACT	20. LIMITATION OF ABSTRACT
UNCLASSIFIED	UNCLASSIFIED	UNCLASSIFIED	SAR

NSN 7540-01-280-5500

Standard Form 298 (Rev. 2-89)
Prescribed by ANSI Std. Z39-18
298-102

CONTENTS

	Page
ABSTRACT	1
ADMINISTRATIVE INFORMATION	1
INTRODUCTION	1
SOLUTION TECHNIQUE	2
NUMERICAL RESULTS	3
NACA 0012 Airfoil	3
NACA 0015 Appendage	10
CONCLUSIONS	22
ACKNOWLEDGMENTS	23
REFERENCES	25

FIGURES

		Page
1.	Coarse grid for the NACA 0012 airfoil.	4
2.	Fine grid for the NACA 0012 airfoil.	4
3.	Y^+ comparison for the NACA 0012 airfoil.	5
4.	Law of the wall comparison for the NACA 0012 airfoil.	6
5.	C_p comparison for the NACA 0012 airfoil.	6
6.	C_f comparison for the NACA 0012 airfoil.	7
7.	Section lift for the forward flow NACA 0012 airfoil.	8
8.	Section drag for the forward flow NACA 0012 airfoil.	8
9.	Section lift for the reverse flow NACA 0012 airfoil.	9
10.	Section drag for the reverse flow NACA 0012 airfoil.	9
11.	Expanded view of the grid near the trailing edge.	10
12.	NACA 0015 configuration and surface grid.	11
13.	Cross section of the NACA 0015 fine grid.	12
14.	Law of the wall comparison for the NACA 0015 appendage.	13
15.	Streamwise velocity contours for the forward flow NACA 0015 appendage.	14
16.	Lift for the forward flow NACA 0015 appendage.	15
17.	Drag for the forward flow NACA 0015 appendage.	15
18.	Lift/Drag for the forward flow NACA 0015 appendage.	16
19.	Moment for the forward flow NACA 0015 appendage.	16
20.	Chordwise center of pressure for the forward flow NACA 0015 appendage.	17
21.	Spanwise center of pressure for the forward flow NACA 0015 appendage.	17
22.	Streamwise velocity contours for the reverse flow NACA 0015 appendage.	18

23. Velocity vectors for the reverse flow NACA 0015 appendage. 19
24. Lift for the reverse flow NACA 0015 appendage. 20
25. Drag for the reverse flow NACA 0015 appendage. 20
26. Lift/Drag for the reverse flow NACA 0015 appendage. 21
27. Moment for the reverse flow NACA 0015 appendage. 21
28. Chordwise center of pressure for the reverse flow NACA 0015. 22
29. Spanwise center of pressure for the reverse flow NACA 0015. 23

ABSTRACT

This report describes efforts to compute forces and moments about an appendage using the Reynolds averaged Navier-Stokes (RANS) equations. All computations presented are done with the Mississippi State University code UNCLE. Calculations are performed for a two-dimensional NACA 0012 airfoil and a three-dimensional NACA 0015 low-aspect ratio appendage mounted on a ground board. Results are presented for both forward and reverse flow conditions.

ADMINISTRATIVE INFORMATION

This work was funded by the Advanced Submarine Research and Development Office (NAVSEA 92R) under the 6.4 Ship Design Tools Project (Project No. F2033), RANS Implementation Task, with internal Work Unit Number 1-2630-707-20. The work described in this report was performed by the Propulsor Department of the Hydromechanics Directorate, Carderock Division, Naval Surface Warfare Center.

INTRODUCTION

There has been much effort in recent years to apply Reynolds Averaged Navier-Stokes (RANS) flow solvers to complex flow fields. The numerical results provide a complete velocity and pressure description around the entire configuration as well as force and moment predictions. Additionally, the computations can provide "pictures" of flow fields by which complex fluid dynamics phenomena can be investigated in more detail than typically available with experiments. Ideally, computations could be used to minimize the amount of experimental testing needed, or they could be done simultaneously with testing to get a more complete description of the flow field. A huge potential area for RANS calculations is the study of Reynolds number effects, particularly as they pertain to full scale versus model scale.

Because of its potential benefit RANS computations are being performed on many relevant hull configurations with multiple appendages.[1, 2, 3] The computations have proven useful for investigating secondary flow features and other effects generated by the hull and appendages. RANS computations provide pressure and velocity data in the entire flow field. However, it is also desirable to obtain the forces and moments generated by the hull and appendages. To obtain force and moment data the computed pressure and stresses must be integrated over the body. Computing the correct pressure drag can be especially difficult on certain geometries as the net drag is a small value obtained by taking the difference of the two large forces generated by the front and stern. The ability of RANS codes to predict to drag of bodies of revolution has recently been looked at by Gorski[4]. Another issue is how well RANS codes can predict the forces and moments generated by the appendages on a typical hull. Although there have been

many wing calculations performed by the aerodynamics community the control surfaces of interest to naval architects is typically of a much lower aspect ratio due to the available space and operating conditions of ships and submarines. As a precursor to using RANS solvers to predict the forces and moments generated by an appended hull configuration the present effort investigates the ability of RANS codes to predict the forces and moments generated by a low-aspect ratio appendage mounted on a ground board which was measured experimentally by Whicker and Fehlner[5]. Calculations are performed at various angles of attack in both forward and reverse flow conditions. The emphasis here is on the forward flow condition, as that is the usual operating condition, but reverse flow calculations are included due to the comparative data being available and the need for this type of information in backing situations.

The RANS code used for the present calculations is the UNCLE code developed at Mississippi State University.[6, 7] This RANS code is being transitioned to the Carderock Division, Naval Surface Warfare Center for propulsor and maneuvering[8, 9] calculations. Consequently, it is a good candidate to evaluate the ability of RANS codes to predict the forces and moments generated by a low-aspect ratio control surface. In addition, to gain experience with the UNCLE code, calculations are shown for a two-dimensional NACA 0012 airfoil measured experimentally by Critzos et al.[10]

SOLUTION TECHNIQUE

The incompressible Reynolds averaged Navier-Stokes equations are solved using the Mississippi State University code UNCLE[6, 7]. The equations are solved using the pseudo-compressibility approach where an artificial time term is added to the continuity equation and then all of the equations are marched in this artificial time till convergence. Only steady state computations are performed as part of this effort. The UNCLE code uses a cell centered finite volume formulation. Thus, dependent variables are stored at cell centers and it is necessary to compute the "fluxes" across the cell faces. The Navier-Stokes equations contain first derivative convective terms and second derivative viscous terms. The viscous terms are numerically well-behaved diffusion terms and are discretized using fairly standard central differences[11]. Only the thin layer approximation to the full Navier-Stokes equations is available in the versions of UNCLE available at CDNSWC at this time. The convective terms are treated using Roe's [12] approximate Riemann solver. A Jacobian matrix is formed for each of the convective flux terms for which eigenvectors and eigenvalues are obtained. By differencing these flux terms based on the sign of the eigenvalues stability can be achieved without any artificial dissipation terms being added to the equations. For the present calculations a third-order upwind biased discretization, based on the MUSCL approach of Van Leer et al.[13], is used for the convective terms. The equations are solved implicitly using a discretized Newton-relaxation method[14] with multigrid techniques implemented for faster convergence[2]. More details of the solver can be found in the various references provided.

The algebraic eddy viscosity model of Baldwin and Lomax[15] is used for turbulence modeling. The Baldwin-Lomax model has been used extensively for airfoil and wing calculations and should be adequate for the present purposes. However, the model is not well suited to predicting the tip vortex which is generated by the appendage which may affect the results somewhat, particularly at high angles of attack where the vortex is strong. This is because it is difficult to compute the correct length scale for the model, which was developed for two-dimensional boundary layers, in such complicated three-dimensional flow regions. As shown by Telste et al.[16], for a similar appendage calculation using the Baldwin-Lomax turbulence model, large eddy viscosity values can arise in the wake far from the vortex core which is also unrealistic. However, it is not known how such difficulties in the wake will influence the integrated force and moment quantities on the appendage itself. Another issue is that the flow may be transitional at the Reynolds numbers investigated here. Although transition regions can be hardwired into the code, or imposed when the eddy viscosity is below a specified minimum, no such ad hoc corrections are attempted here.

The boundary conditions imposed are rather straight forward. Standard no-slip boundary conditions are imposed on the airfoil and appendage surfaces. No attempt is made to model the tunnel walls in either experiment replicated here since tunnel wall corrections were applied to both sets of documented data by the original authors performing the experiments. Consequently, far field free-stream boundary conditions are imposed using the non-reflecting characteristic boundary conditions available in UNCLE. For the three-dimensional appendage experiment the appendage is mounted on a ground board with a gap between the appendage and ground board. No attempt is made to model this gap or the boundary layer on the ground board as they are believed to minimally affect the forces generated by the appendage. Thus, the appendage is modeled as if it extends all the way to the ground board, without the gap, and standard reflection boundary conditions imposed on the ground board.

NUMERICAL RESULTS

NACA 0012 Airfoil

Calculations for the two-dimensional NACA 0012 section correspond to a Reynolds number of 1.8×10^6, based on chord, at angles of attack from 0^o to 20^o. Comparisons are made with the experimental data of Critzos et al.[10] At this Reynolds number there may be transitional effects in the experiment because the airfoil was polished to a high degree of smoothness, but this is not taken into account in the calculations. Two different O-grids are used with the outer boundary 20 chord lengths away from the airfoil. One grid is "coarse" with 121 points wrapping around the airfoil and 41 points extending out from it, Fig. 1, and a second "fine" grid which has 161 points wrapping around the airfoil and 81 points normal to it, as shown in Fig. 2. The main difference between the two grids is the boundary layer resolution with the fine grid having the first point off of

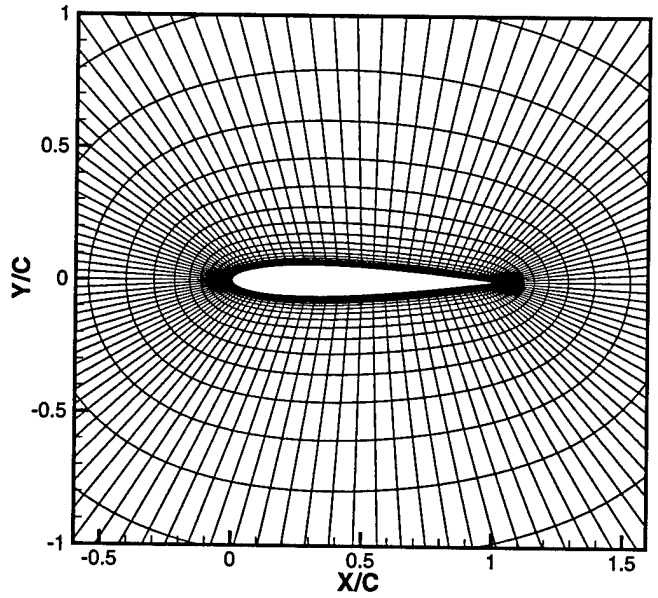

Fig. 1. Coarse grid for the NACA 0012 airfoil.

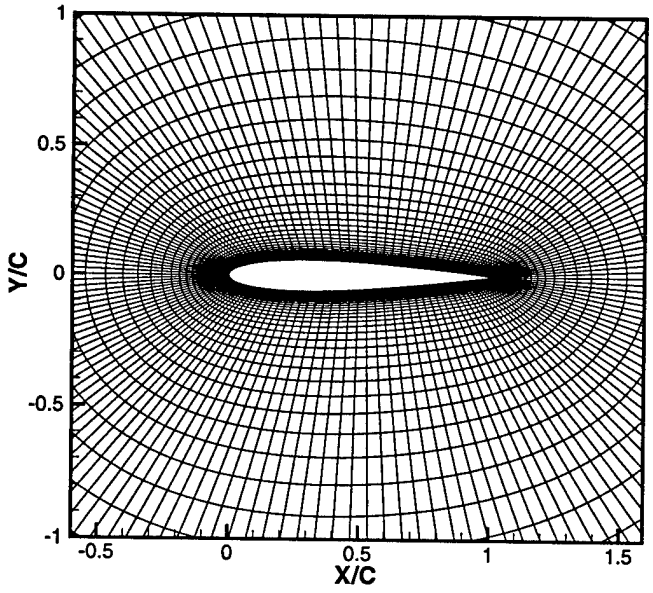

Fig. 2. Fine grid for the NACA 0012 airfoil.

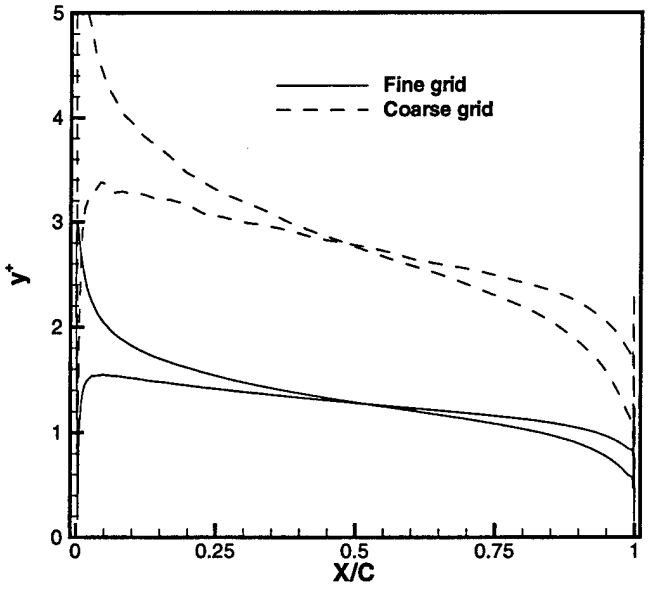

Fig. 3. Y^+ comparison for the NACA 0012 airfoil.

the wall at around y^+ of 1 or 2 and the coarse grid having y^+ values around 3. Shown in Fig. 3 is the y^+ distribution of the first centroid off of the wall, for the two grids, at a 4^o angle of attack. The clustering towards the airfoil is different with the fine grid having significantly more points in the boundary layer. However, the differences in the grid have little impact on the overall results. A typical profile in wall coordinates is shown in Fig. 4 for the two grids. Also plotted in this figure is the law of the wall formula of Spalding[17]. Spalding's[17] formula smoothly transitions from the inner layer, where the linear law applies, to the outer layer where the law of the wall equation applies. As can be seen, the computed profiles compare very well with Spalding's equation throughout the boundary layer and there are only minor differences between the coarse and fine grid results. A comparison of pressure coefficient, C_p, and skin friction, C_f, Figs. 5 and 6 respectively, also show little difference between the two grids at 4 degrees angle of attack. These small differences do not translate into significant differences when the lift and drag are computed. As seen in Fig. 7 the predicted section lift coefficient is in very good agreement with the data of Critzos et al.[10] out to an angle of attack of almost 16 degrees. However, at approximately 16 degrees the experimental data indicates stall occurs with a rapid drop in lift. The computations do not predict this stalled behavior even out to 20 degrees. This may be due to the standard Baldwin-Lomax turbulence model being used and would need further work to clarify. It does not seem to be due to grid dependence since both the coarse and fine grids give much the same result. The computed section drag coefficient is shown in Fig. 8. Here only a comparison of the

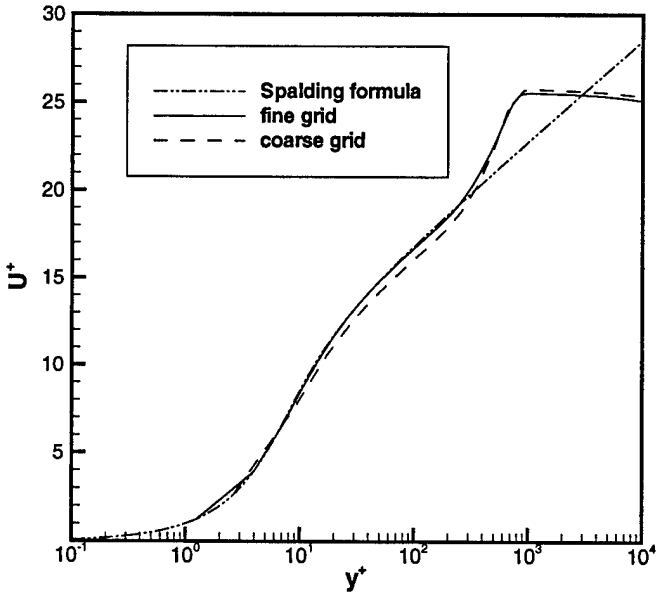

Fig. 4. Law of the wall comparison for the NACA 0012 airfoil.

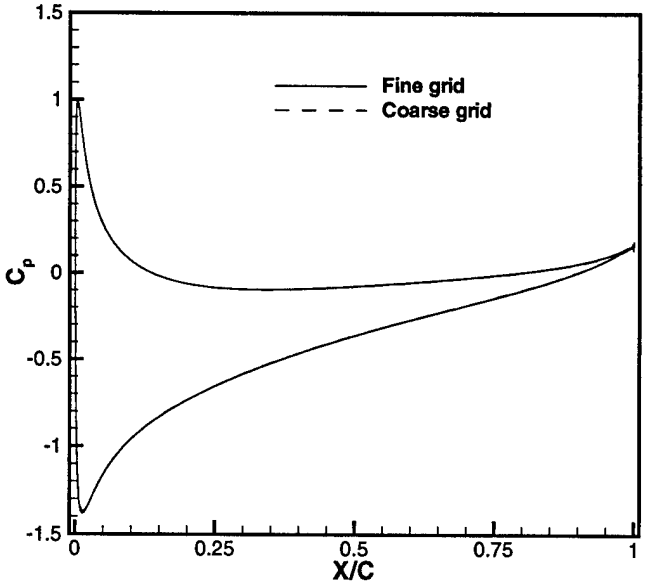

Fig. 5. C_p comparison for the NACA 0012 airfoil.

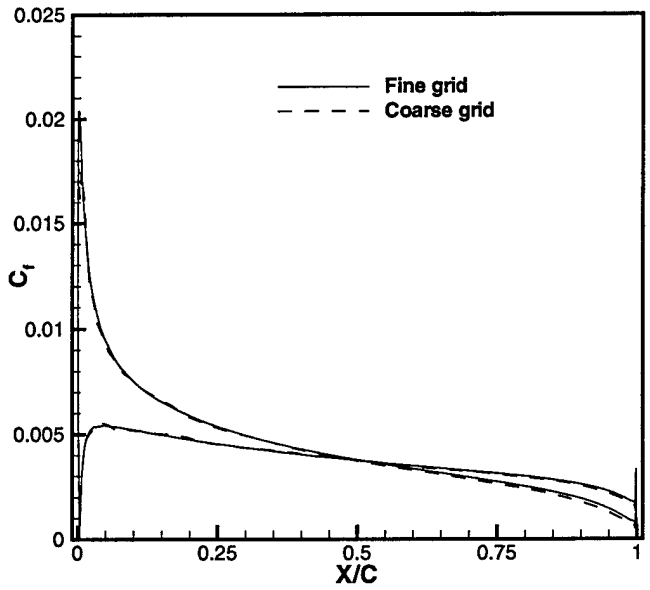

Fig. 6. C_f comparison for the NACA 0012 airfoil.

coarse and fine grid computations is shown as accurate experimental values could not be obtained from the experimental report. Again there is not much difference in the solutions due to the different grids.

Computations are also performed for the airfoil in reverse flow conditions. Again the Reynolds number is 1.8 x 10^6, based on chord, and the same grids are used as in the forward flow conditions. Here the section lift coefficient is not as well predicted as for the forward flow case as show in in Fig. 9. The reverse flow condition presents a more difficult problem because of the inherent flow separation at the rear and the thin leading edge of the blade at the front which will affect the computed lift. Although it appears that the grid resolution is not the issue, since both coarse and fine grids give nearly the same results for section lift and drag (Fig. 10), there may be a problem that the trailing edge of the blade (which becomes the leading edge for reverse flow conditions) is not resolved well enough for this calculation. Shown in Fig. 11 is an expanded view of the fine grid near the trailing edge of the blade. It may be that by putting more points around the airfoil the pressure rise would be computed more accurately leading to better lift predictions. However, this grid is typical of what would be used for an airfoil calculation.

Resolving the issues regarding reverse flow calculations is beyond the scope of this work. These calculations merely point out that the reverse flow condition may be more difficult to compute accurately than the standard forward flow condition and care should be exercised when computing such conditions. There is also the possibility that

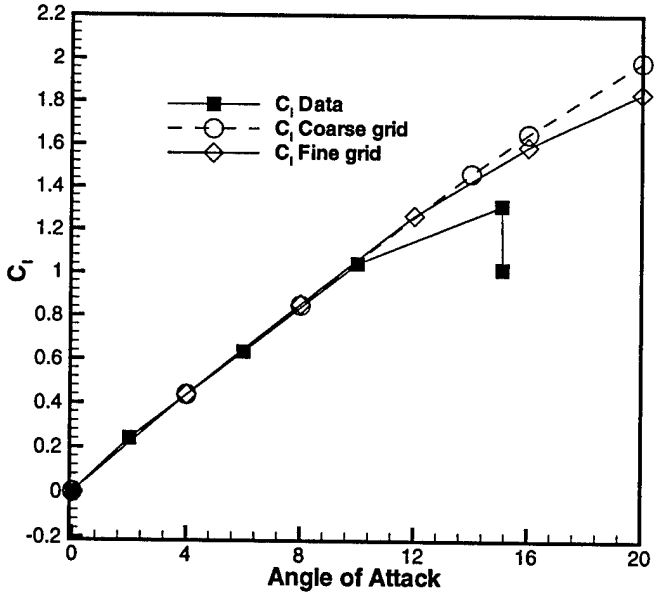

Fig. 7. Section lift for the forward flow NACA 0012 airfoil.

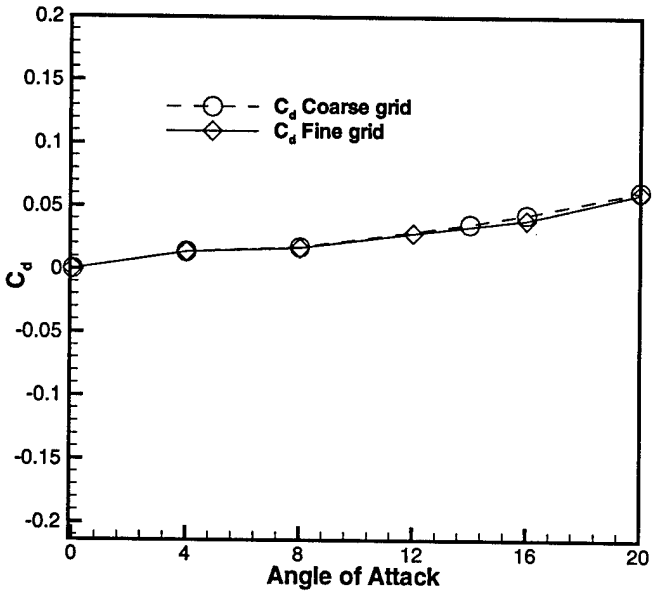

Fig. 8. Section drag for the forward flow NACA 0012 airfoil.

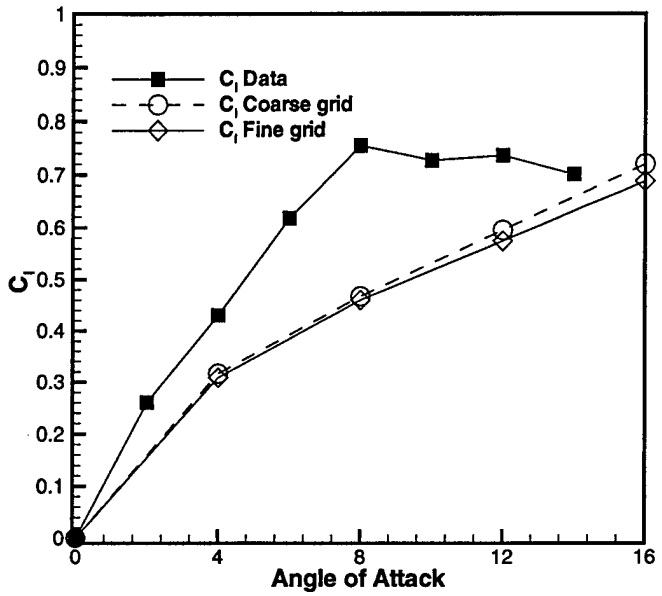

Fig. 9. Section lift for the reverse flow NACA 0012 airfoil.

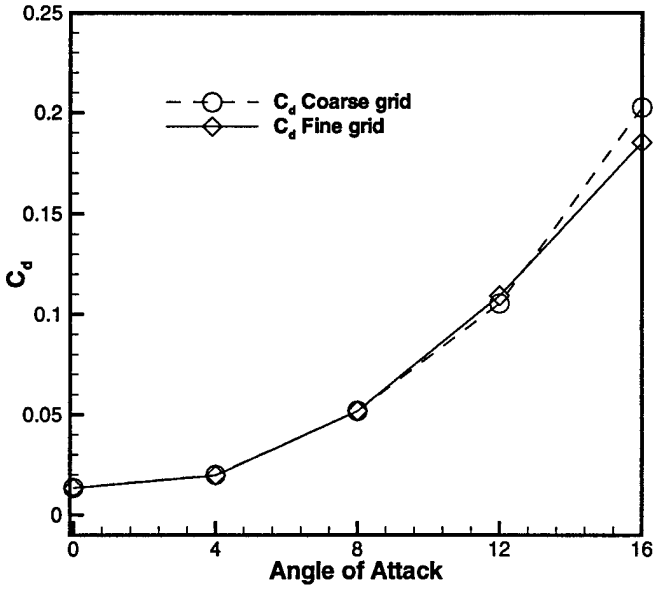

Fig. 10. Section drag for the reverse flow NACA 0012 airfoil.

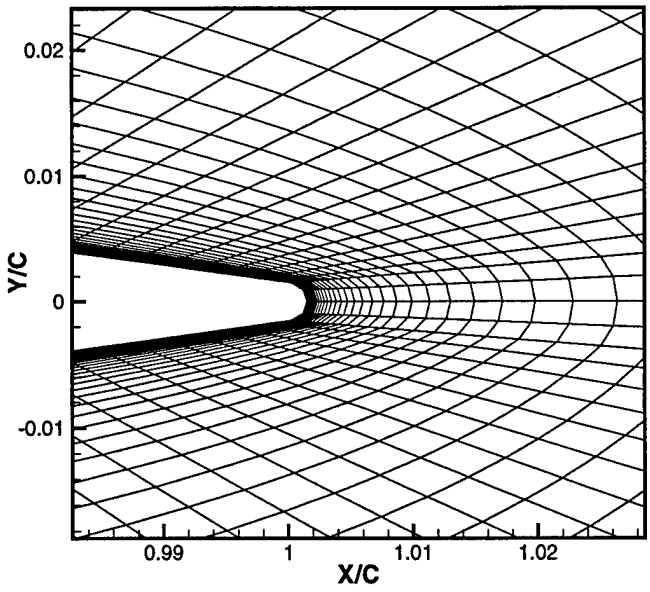

Fig. 11. Expanded view of the grid near the trailing edge.

laminar to turbulent flow transition is affecting the data. Critzos et al.[10] also performed experiments in the reverse flow condition at a Reynolds number of 0.5 x 10^6. For this condition they showed discontinuities in the lift around 0 degrees angle of attack. They postulated this was due to laminar separation bubbles forming and the flow becoming fully turbulent only after the flow reattached. If this is correct the 1.8 x 10^6 case may also be undergoing such transitional effects, but not as severe as the lower Reynolds number case. Again it is worth mentioning that the airfoil is modeled as being fully turbulent and such transition effects are not predicted by the computation.

NACA 0015 Appendage

A three-dimensional appendage has also been computed corresponding to a family of all-movable, low-aspect ratio control surfaces which were experimentally investigated by Whicker and Fehlner[5]. The force and moment coefficients and chordwise and spanwise centers of pressure were presented as functions of angle of attack. Various different models were tested by Whicker and Fehlner[5] to examine the effect of aspect ratio, sweep angle, tip shape, and section shape. The models were run in both forward and reverse flow conditions. Tests were performed in a 8 ft. (2.44 m) by 10 ft. (3.05 m) wind tunnel with a Reynolds number range of 1 to 3 million based on the mean chord length. The control surfaces were mounted within the wind tunnel on a ground board with a gap of 1/8 inch (0.32 cm) between the root of the control plane and the board. Measurements were taken using a motor-driven, null-type, mechanical balance

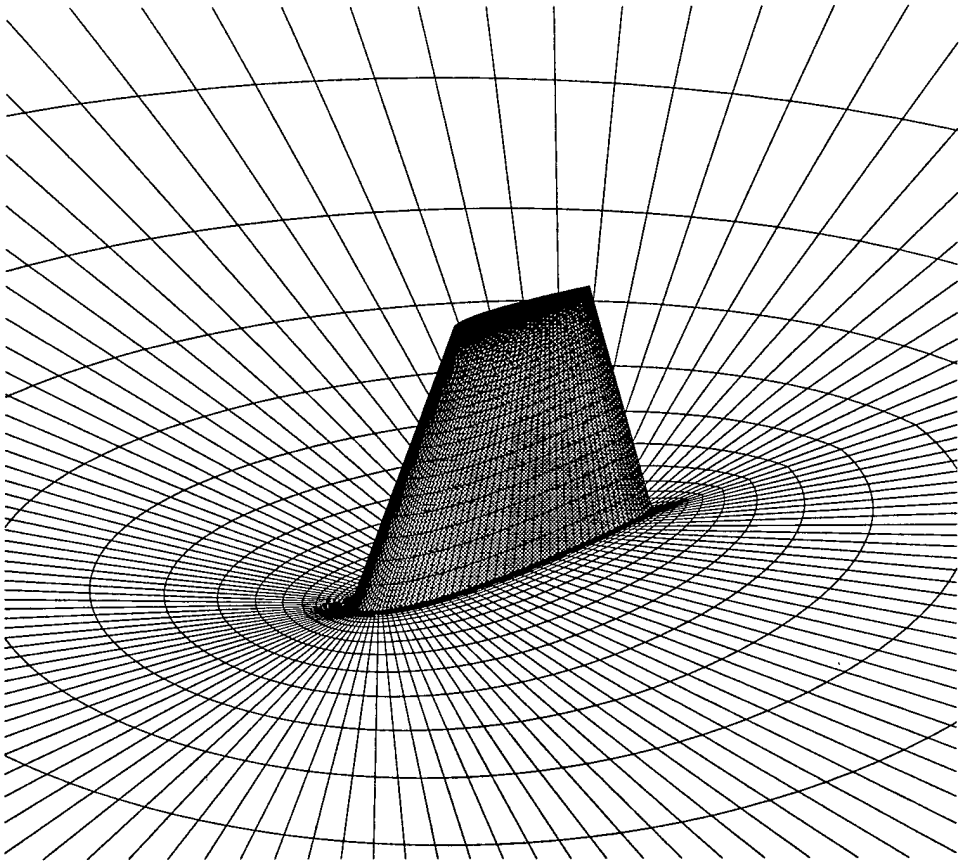

Fig. 12. NACA 0015 configuration and surface grid.

and accuracy was reported as: lift, ± 0.2 lbs.; drag, ± 0.1 lbs.; and moment, ± 0.1 ft-lbs.

Of this family, model AM106 is numerically modeled for this report. Model AM106 is a NACA 0015 section control surface with an effective aspect ratio of 2, a sweep angle of 11 degrees, a semi-span of 2 feet (0.61 m), and a squared off tip. The flow is computed at the maximum Reynolds numbers tested of 2.72 million for the forward flow cases and at 3.0 million for the reverse flow.

The appendage configuration and surface grid is shown in Fig. 12. Looking at a two-dimensional cross section, Fig. 13, an O-grid much like that for the NACA 0012 airfoil calculation is used. Again both coarse and fine grids are used. The fine grid consists of 121 points around the appendage in the chordwise direction, 41 points normal to the appendage for boundary layer resolution, and 67 points in the spanwise direction where 41 of these 67 points are on the appendage itself and the other 25 points extend from the tip out to the far field. These 25 points extending out to the far field wrap around a "cap" block of grid points which covers the tip of the appendage. The grid is fanned out as it moves away from the foil to provide good resolution near the tip and larger, more computationally efficient cells towards the far field. The "coarse" grid is basically the same grid, but every other point wrapping around the appendage in the chordwise

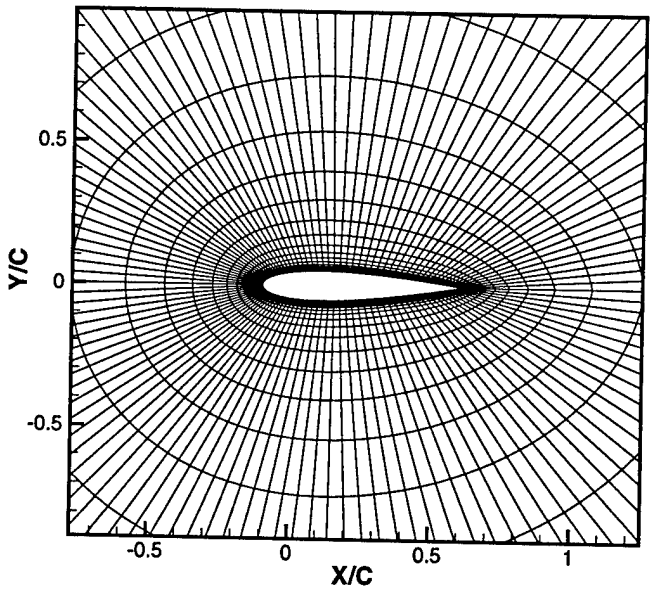

Fig. 13. Cross section of the NACA 0015 fine grid.

direction is removed providing only 61 points wrapping around the appendage. This type of coarse grid resolution is more consistent with the gridding that is done for an appendage as part of a complete ship or submarine calculation. The grid distribution normal to the wall does not change between the two grids. The distance from any no slip surface to the first point off the wall is specified to be less than 0.0001 units. This gives enough resolution so that the first point off of the wall is generally within a y^+ value of 1. As shown in Fig. 14, for some representative velocity profiles at approximately midspan and midchord, the agreement with Spalding's[17] equation is quite good showing there is sufficient boundary layer resolution with the grids.

Streamwise velocity contours for the 8 degree angle of attack case are shown in Fig. 15 which is typical of the flow fields predicted. A tip vortex is formed where the strength largely depends on the angle of attack. The downstream wake is wider on the suction side than on the pressure side. The wake thickness also varies over the span due to different section chord length and thickness. The wake also thins considerably near the tip of the appendage due to the presence of the tip vortex. The lift, drag, and corresponding lift/drag predictions for the forward flow case are shown in Figs. 16, 17, and 18, respectively. There is not much difference between the coarse and fine grid results for the drag, but for the lift prediction there is some discrepancy above 8^o with the coarse grid calculations producing more lift than the fine grid. However, the computed lift and drag, particularly with the fine grid, are in very good agreement with the experimental data out to 28 degrees. There again may be some overprediction of

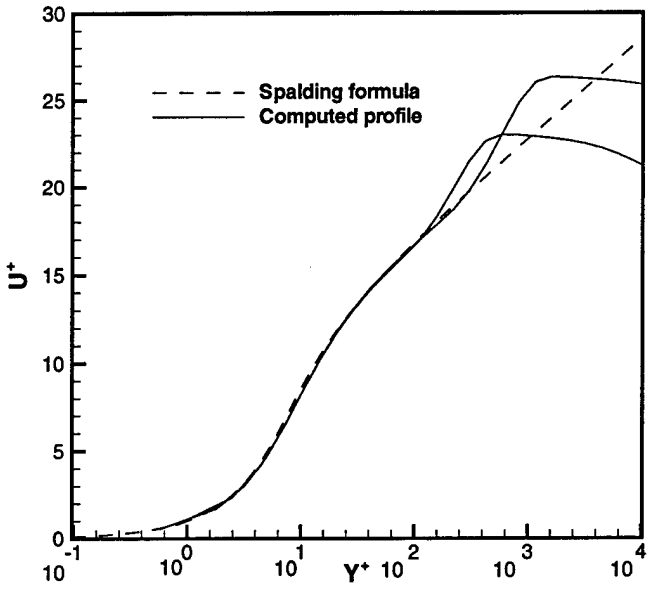

Fig. 14. Law of the wall comparison for the NACA 0015 appendage.

stall with the computations as the experimental lift starts to drop off beyond 28 degrees while the computed lift slope remains fairly constant. Again, no special provisions are made to the Baldwin-Lomax turbulence model to better account for separated flow or the tip vortex generated for this three-dimensional case. The moment is also quite well predicted with a slight drop off in the prediction beyond 12 degrees as seen in Fig. 19. Here the moment is about the quarter-chord point of the mean geometric chord. The chordwise center of pressure, $(CP)_c$, which was measured from the leading edge at mean geometric chord in percent of the mean geometric chord, is also well predicted by the calculation as shown in Fig. 20. The values themselves are a little high, but the same slope as the experimental data is obtained with both the coarse and fine grids. The spanwise center of pressure, $(CP)_s$, which was measured from the plane of the root section in percent of semispan, is also well predicted by the calculation as shown in Fig. 21. In fact, the predicted spanwise center of pressure is considerably better than that predicted using elliptic loading theory which is also shown in the figure.

Overall the forward flow calculations are in very good agreement with the experimental data out to large angles of attack. The only discrepancies are near stall conditions. In a more recent study Lewandowski[18] tested a series of control surfaces and compared two of them to the data of Whicker and Fehlner[5]. The two sets of data were for the same NACA 0015 sections with aspect ratios of 1.0 and 1.5, but the measurements of Lewandowski are at a lower Reynolds number. The measured lift between the different sets of experimental data compared very well out to approximately 10 degrees angle of

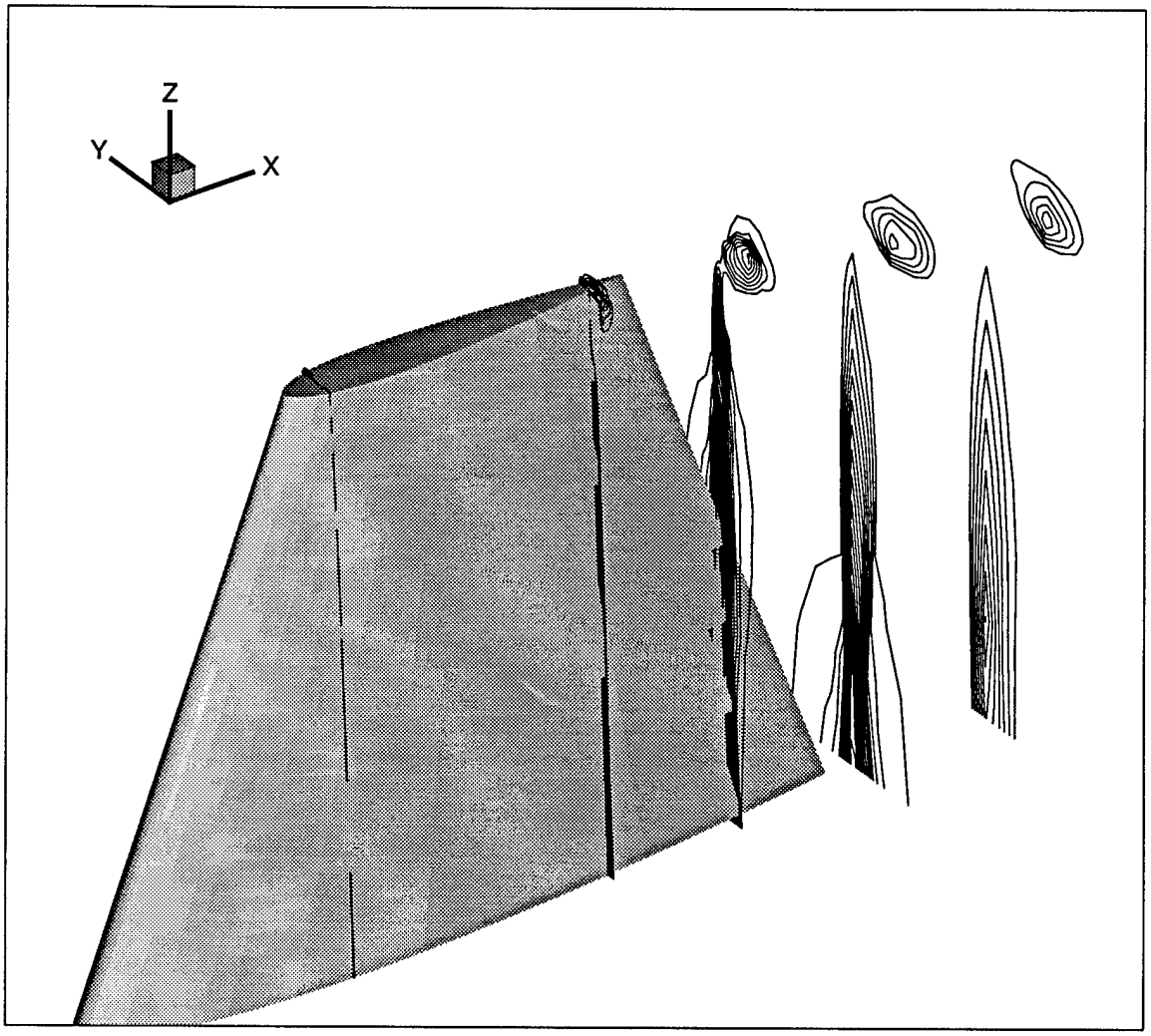

Fig. 15. Streamwise velocity contours for the forward flow NACA 0015 appendage.

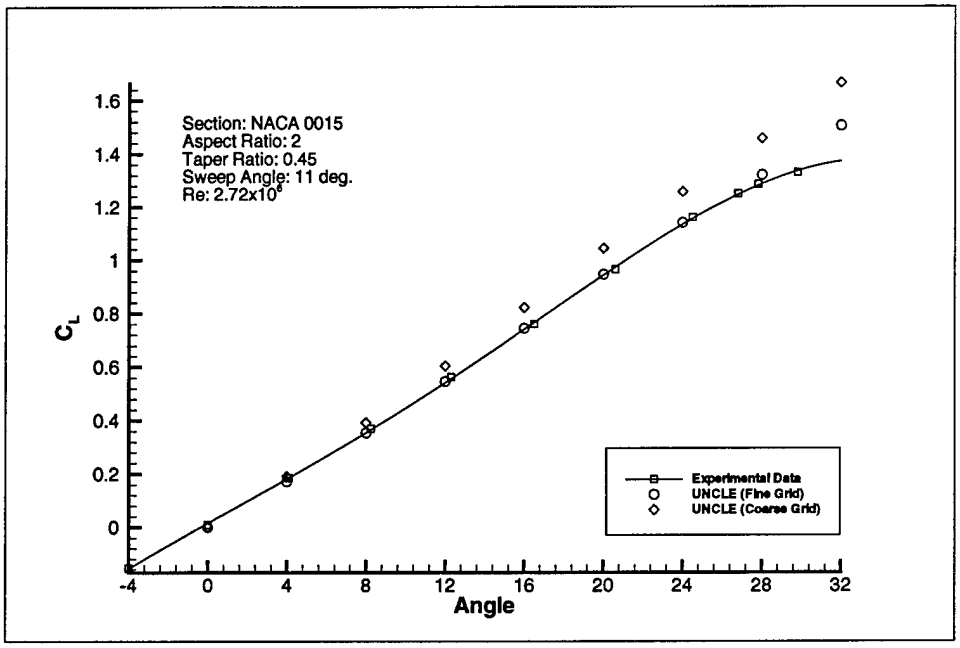

Fig. 16. Lift for the forward flow NACA 0015 appendage.

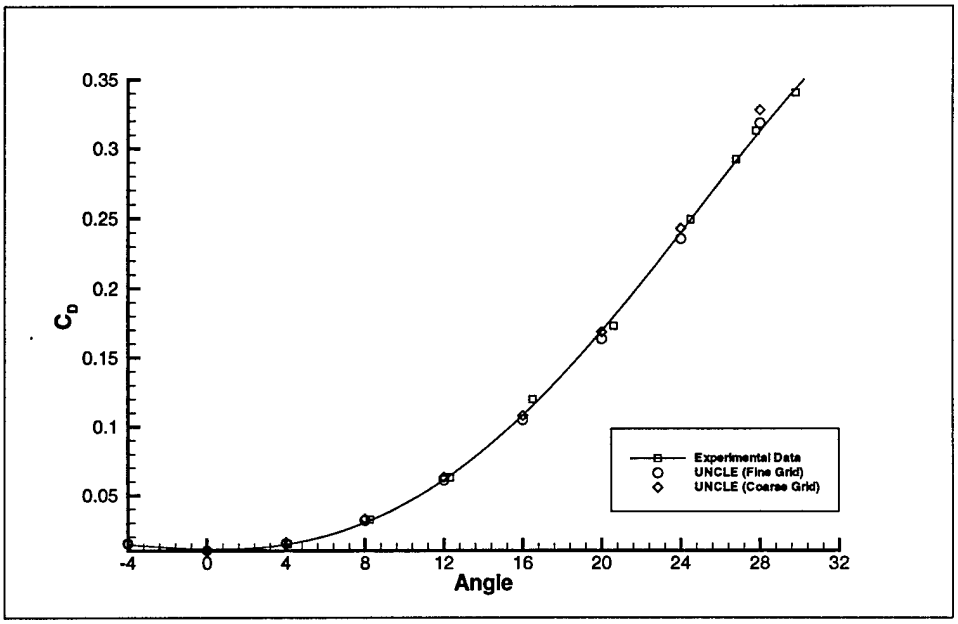

Fig. 17. Drag for the forward flow NACA 0015 appendage.

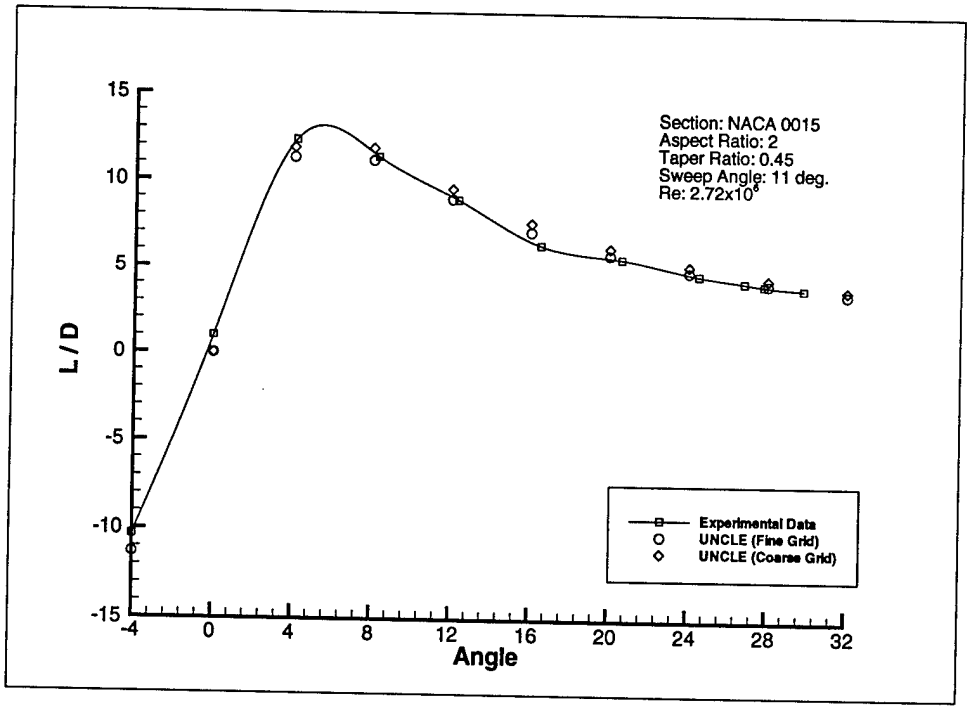

Fig. 18. Lift/Drag for the forward flow NACA 0015 appendage.

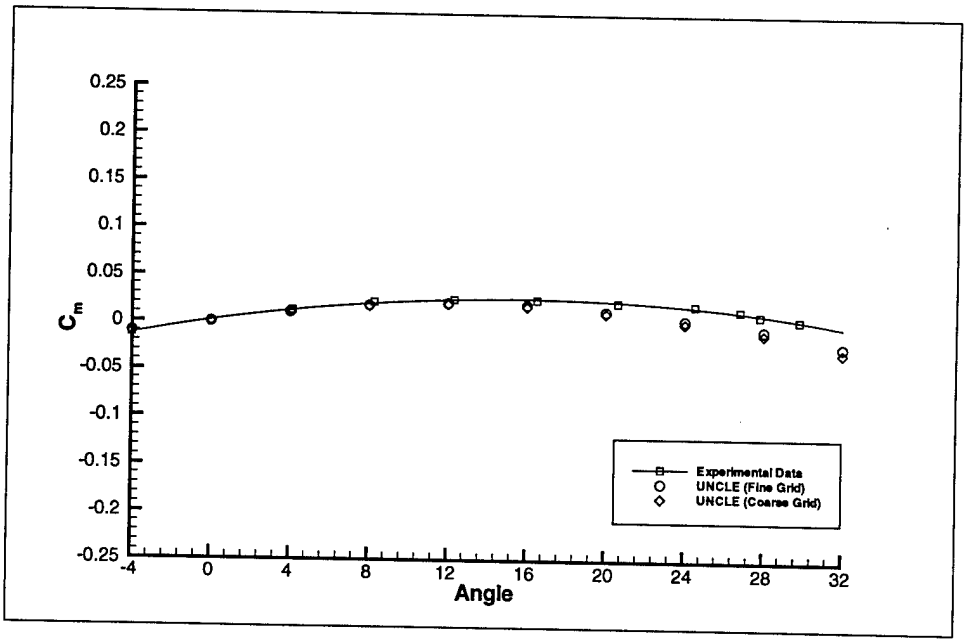

Fig. 19. Moment for the forward flow NACA 0015 appendage.

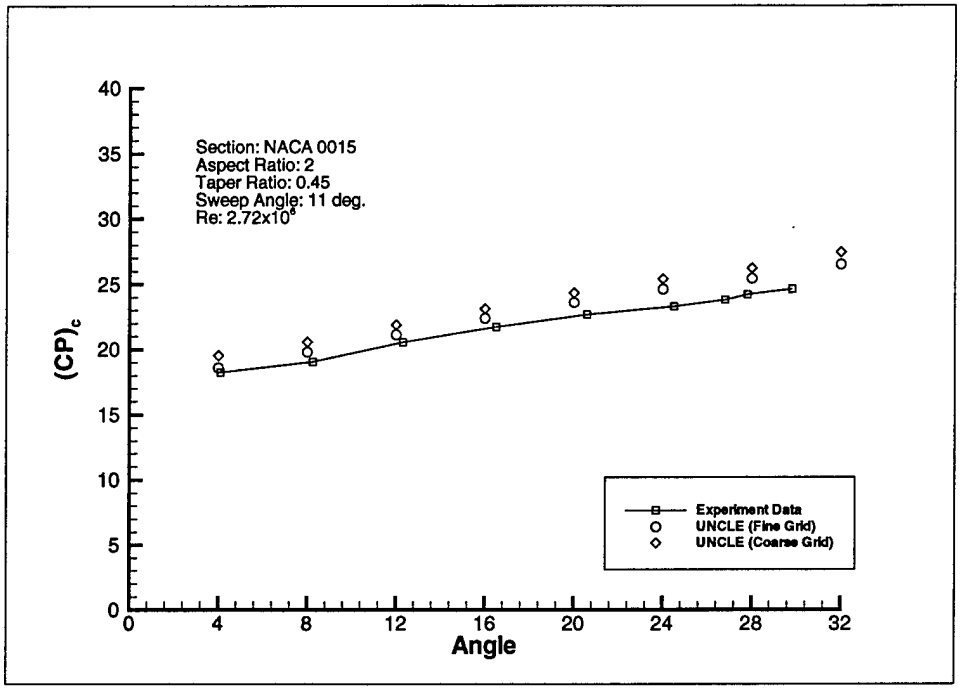

Fig. 20. Chordwise center of pressure for the forward flow NACA 0015 appendage.

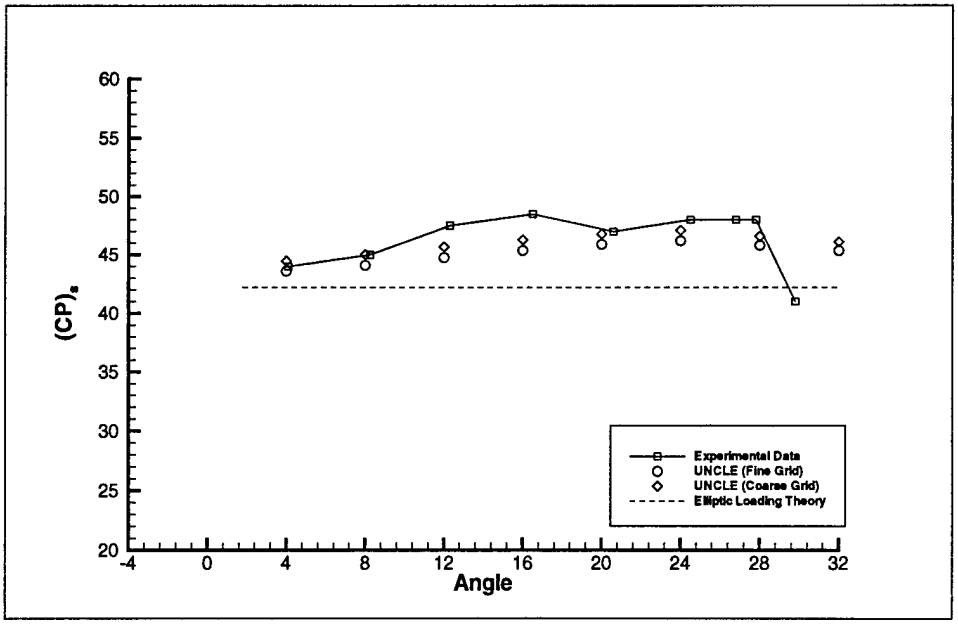

Fig. 21. Spanwise center of pressure for the forward flow NACA 0015 appendage.

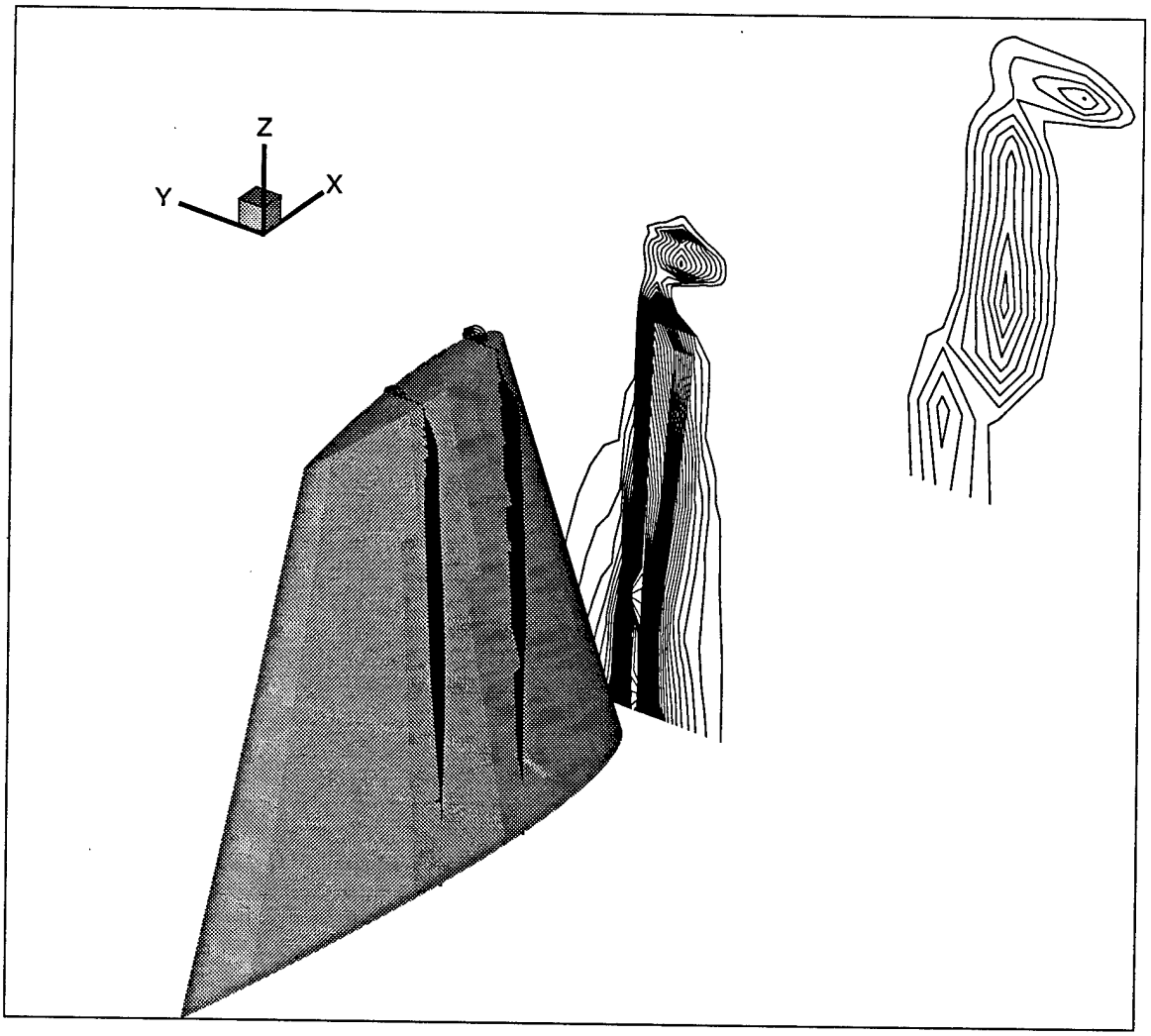

Fig. 22. Streamwise velocity contours for the reverse flow NACA 0015 appendage.

attack indicating little dependence on Reynolds number at angles of attack below stall. However, at angles of attack approaching stall there is considerable difference between the experimental data of Lewandowski[18] and that of Whicker and Fehlner[5] with the low Reynolds number experiment generating significantly less lift than the higher Reynolds number experiment. Such Reynolds number dependence may be one explanation why the calculations, which ignore transition, predict the experimental data very well below stall, but tend toward high values near stall.

For the reverse flow conditions the same grids are used as for the forward flow calculations. Streamwise velocity contours for the 8 degree angle of attack case are shown in Fig. 22. There are some differences between this and the forward flow case. Again a tip vortex is formed, but it is interesting to note that here there is more vortex generation on top of the appendage where as for the forward flow it formed more to the side. The tip vortex formed in the reverse flow condition is generally larger than

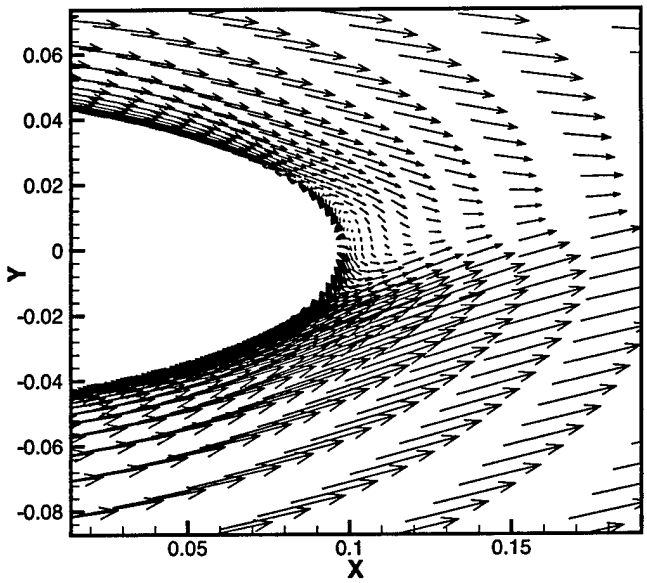

Fig. 23. Velocity vectors for the reverse flow NACA 0015 appendage.

that formed for the forward flow. Another difference is the much wider wake produced by the reverse flow case. It is expected that this wider wake leads to stronger viscous effects. As seen by the velocity vectors for the 8 degree case, Fig. 23, the flow is quite complicated at the rear due to its bluntness. The lift, drag, and corresponding lift/drag predictions for the reverse flow are shown in Figs. 24, 25, and 26, respectively. There is considerably more discrepancy here between the calculations and experiments than seen for the forward flow case. The lower angles of attack are predicted reasonably well, but beyond 12 degrees the lift and drag are underpredicted by the computation. The moment is fairly well predicted even at 12 degrees angle of attack, Fig. 27, but falls off beyond that. Again there is little difference between the coarse and fine grid predictions for these quantities. What is interesting to note is that even below 12 degrees where the lift, drag, and moment are predicted reasonably well the chordwise center of pressure is poorly predicted as show in Fig. 28. The reverse flow chordwise center of pressure is computed from the lift, drag, and moment using

$$(CP)_c \;=\; 0.75 - \frac{C_m}{C_L cos\alpha + C_D sin\alpha}$$

where α is the angle of attack. At small angles of attack the lift contribution dominates over the drag contribution in this expression. It is felt that the negative values predicted beyond 8 degrees are due to the underprediction of lift for these angles of attack even though the moment is well predicted. The predicted spanwise center of pressure is at least similar to that measured experimentally, Fig. 29, but the differences in slope

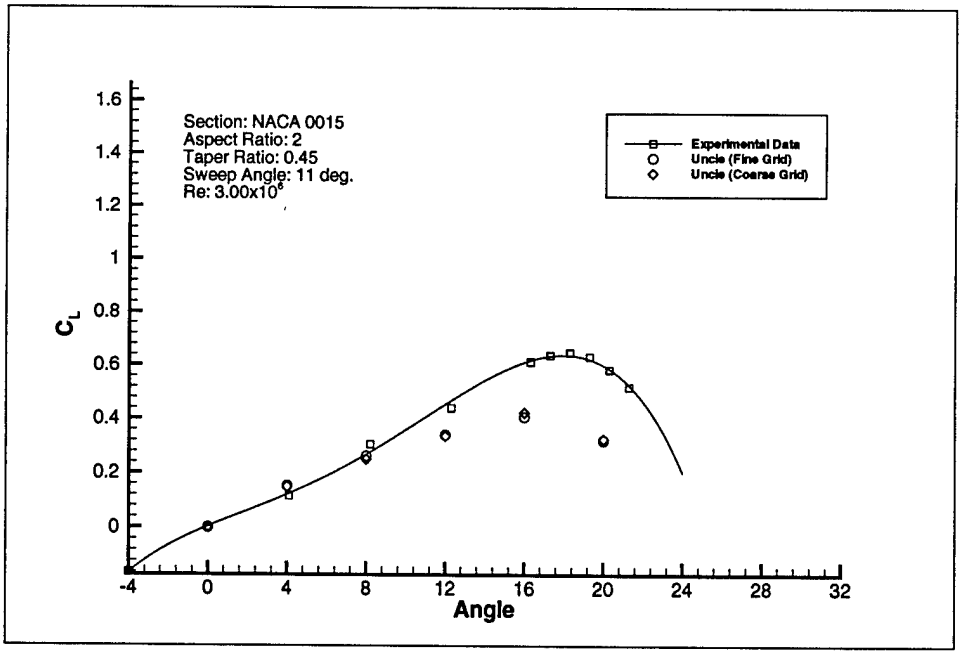

Fig. 24. Lift for the reverse flow NACA 0015 appendage.

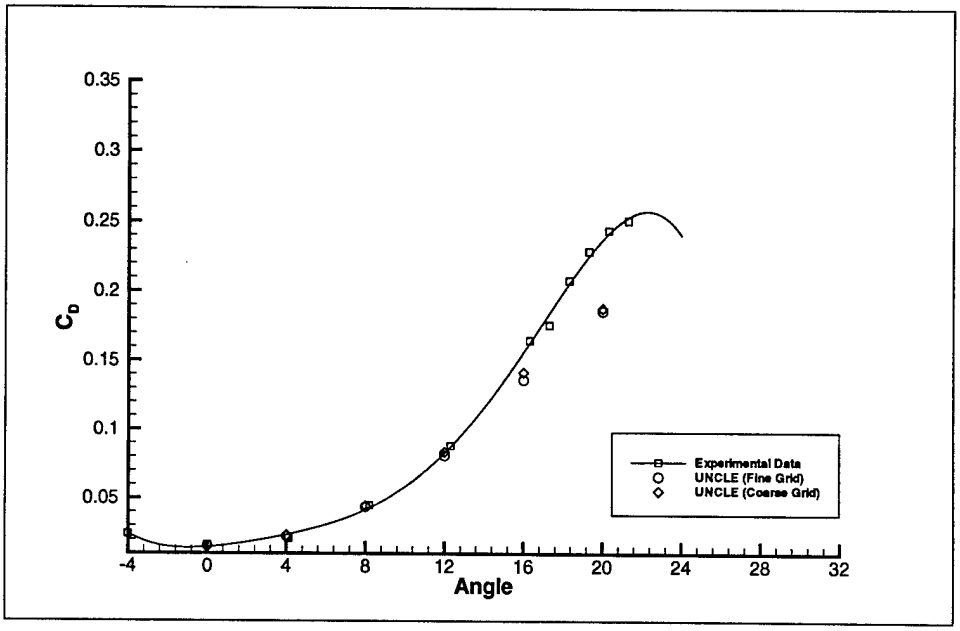

Fig. 25. Drag for the reverse flow NACA 0015 appendage.

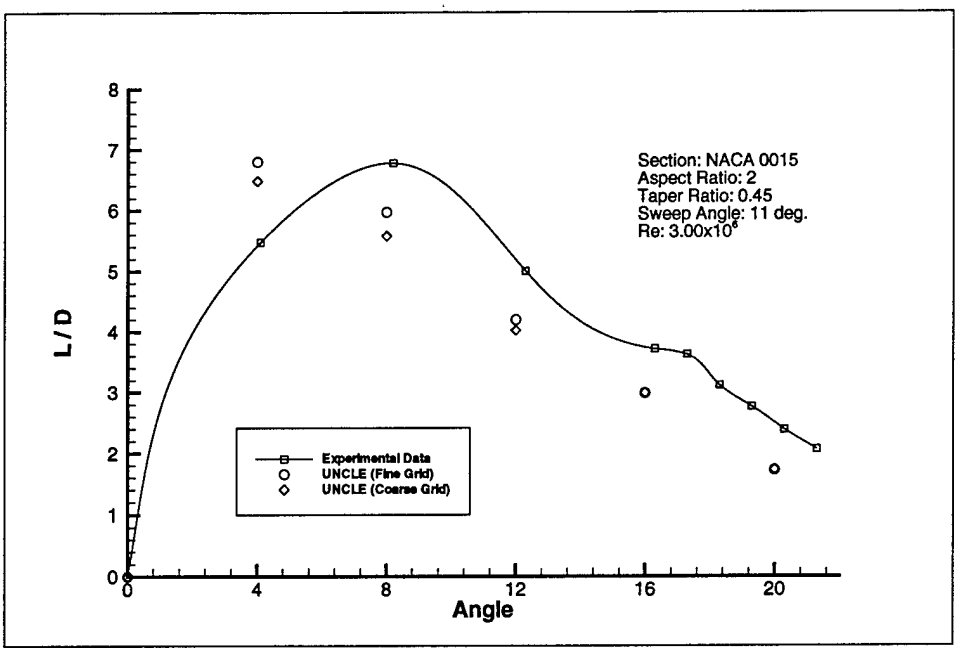

Fig. 26. Lift/Drag for the reverse flow NACA 0015 appendage.

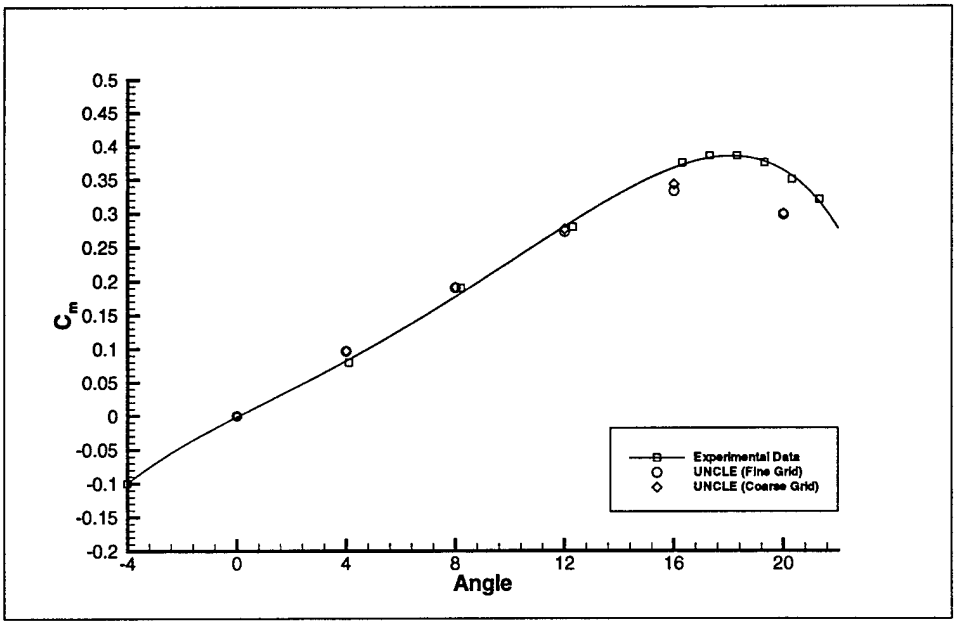

Fig. 27. Moment for the reverse flow NACA 0015 appendage.

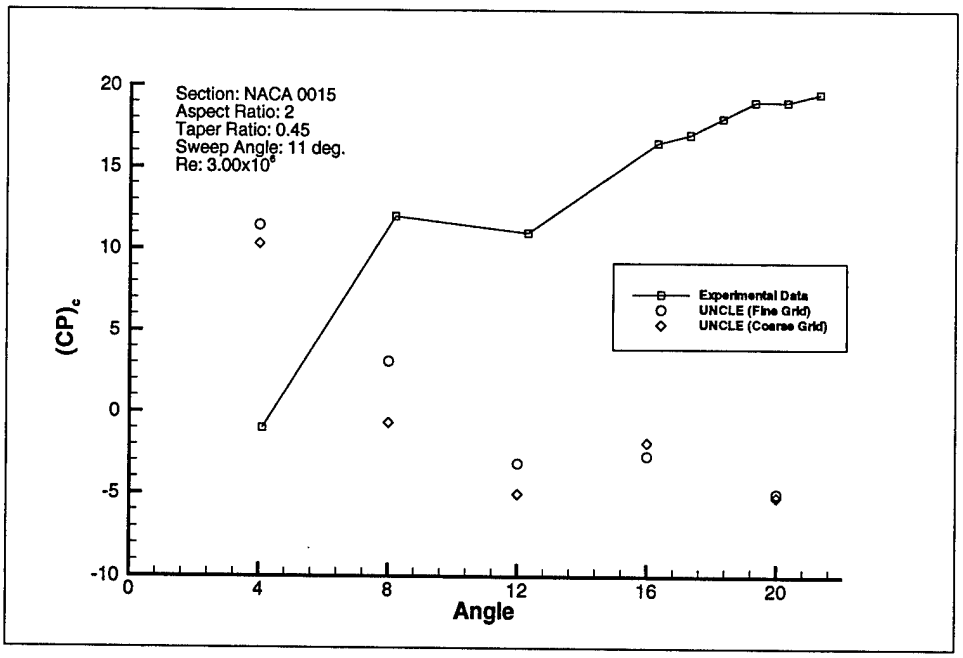

Fig. 28. Chordwise center of pressure for the reverse flow NACA 0015.

are reason for concern. The authors believe they have made no errors in computing these centers of pressure from the computations. As with the two-dimensional airfoil calculations discussed previously there may not be adequate resolution at the trailing edge to properly predict some of the effects generated with the flow in reverse. However, there is not a lot of difference between the coarse and fine grid results indicating all the discrepancies are not purely due to inadequate grid resolution.

CONCLUSIONS

As already mentioned, RANS computations are being used for fully appended ship and submarine configurations. These computations provide force and moment estimates. The intent of this work is to determine how reliably such RANS computations can provide force and moment estimates for individual low-aspect ratio appendages relevant to the Navy community. To this end calculations are demonstrated using the RANS code UNCLE, developed at the Mississippi State University, for a two-dimensional NACA 0012 airfoil at a Reynolds number of 1.8 x 10^6 and a low-aspect ratio NACA 0015 appendage, mounted on a groundboard, with a Reynolds number of approximately 3.0 x 10^6. These calculations correspond to the experimental data of Critzos et al.[10] and Whicker and Fehlner[5]. Grid resolutions are typical of what is used to grid an individual appendage region of a fully appended ship or submarine configuration. For the forward flow conditions, which are the main concern of this effort, the RANS code provided good agreement with the experimental data for lift, drag, moment, and centers of pressure at angles of attack out to stall conditions. The

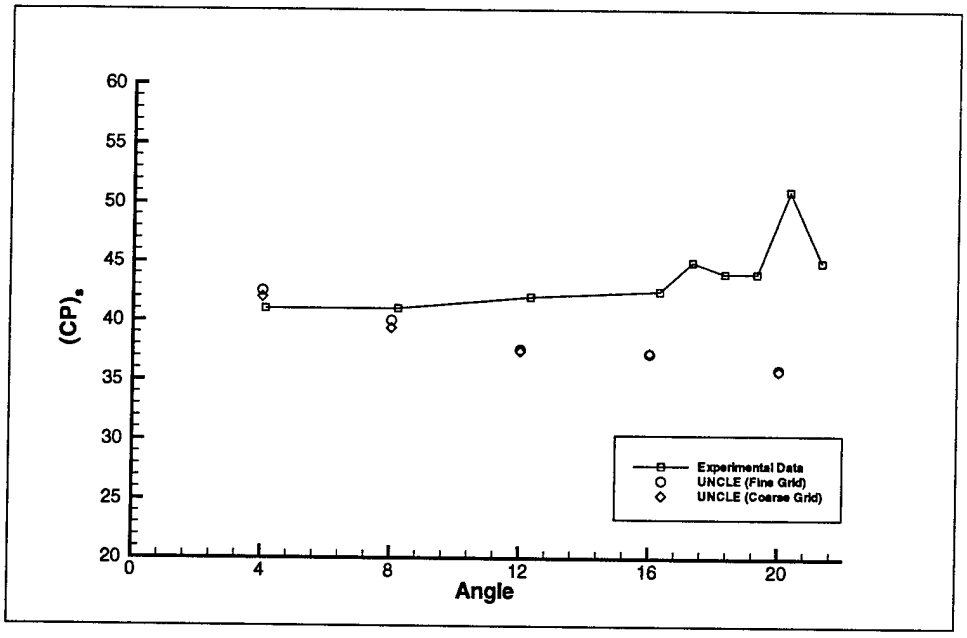

Fig. 29. Spanwise center of pressure for the reverse flow NACA 0015.

fact that good agreement is obtained at 28 degrees angle of attack for the NACA 0015 appendage is very encouraging. The one area of concern is that stall does not appear to be correctly predicted with the calculations overestimating lift near angles of attack where stall occurs. There are a number of possibilities for this including transitional and tunnel wall effects in the experiments, turbulence modeling and grid resolution, to name a few, but resolving this issue is beyond the scope of the current effort.

Due to some recent interest in applying RANS computations to such complicated reverse flow conditions as crashback[3] reverse flow calculations are also done. The same grids used for the forward flow conditions are also used for reverse flow. The results are not generally as good as for the forward flow conditions, but the lift, drag, and moment calculations are reasonably predicted out to 8 to 12 degrees angle of attack. Beyond that the computations underpredict the experimentally measured values. The centers of pressure are not well predicted, even at the low angles of attack, which is some indication of the sensitivity of these quantities. These results do not mean that RANS calculations cannot accurately predict the reverse flow case, but merely that the reverse flow condition may be more difficult to compute accurately than the standard forward flow condition and care should be exercised when computing such conditions.

ACKNOWLEDGMENTS

The authors would like to thank Dr. Lafayette Taylor for his helpful advice on using the UNCLE code during this program. In addition, this work was supported in part by grants of computer time from the U.S. Navy Hydrodynamic/Hydroacoustics Technology Center and the DoD HPC Center at the Naval Research Laboratory.

REFERENCES

1. Gorski, J. J., R. M. Coleman, and H. J. Haussling, "Computation of Incompressible Flow Around DARPA SUBOFF Bodies," DTRC Report No. 90/016, (June 1990).

2. Sheng, C., L. Taylor, and D. Whitfield, "Multiblock Multigrid Solution of Three-Dimensional Incompressible Turbulent Flows About Appended Submarine Configurations," AIAA Paper No. 95-0203, (Jan. 1995).

3. Zierke, W. C. (ed.), "A Physics-Based Means of Computing the Flow Around a Maneuvering Underwater Vehicle," The Pennsylvania State University, Applied Research Laboratory, Technical Report No. TR 97-002, (Jan. 1997).

4. Gorski, J. J., "Drag Calculations of Unappended Bodies of Revolution," CRDKNSWC/HD-1362-07, (May 1998).

5. Whicker, L. F. and L. F. Fehlner, "Free-Stream Characteristics of a Family of Low-Aspect-Ratio, All-Movable Control Surfaces for Application to Ship Design," David Taylor Model Basin Report 933, (Dec. 1958).

6. Taylor, L. K. and D. L. Whitfield, "Unsteady Three-Dimensional Incompressible Euler and Navier-Stokes Solver for Stationary and Dynamic Grids," AIAA Paper No. 91-1650, (June 1991).

7. Taylor, L. K., A. Arabshahi, and D. L. Whitfield, "Unsteady Three-Dimensional Incompressible Navier-Stokes Computations for a Prolate Spheroid Undergoing Time-Dependent Maneuvers," AIAA Paper No. 95-0313, (Jan. 1995).

8. Busby, J. A., "Evaluation of the Mississippi State University Computational Fluid Dynamics Code (UNCLE)," CRDKNSWC-HD-1318-01, (Sept. 1996).

9. Haussling, H. J., "Transition and Testing at CDNSWC of the UNCLE.6DOF Submarine Maneuvering Code," CRDKNSWC/HD-1318-02, (Nov. 1997).

10. Critzos, C. C., H. H. Heyson, and R. W. Boswinkle, "Aerodynamic Characteristics of NACA 0012 Airfoil Section at Angles of Attack from 0° to 180°," NACA TN 3361 (1954).

11. Gatlin, B., "An Implicit Upwind Method for Obtaining Symbiotic Solutions to the Thin-Layer Navier-Stokes Equations," Ph.D. Dissertation, Mississippi State University, (Aug. 1987).

12. Roe, P. L., "Approximate Riemann Solvers, Parameter Vectors, and Difference Schemes," *J. of Comp. Physics,* Vol. 43, pp. 357-372, (May 1981).

13. Van Leer, B., J. L. Thomas, P. L. Roe, and R. W. Newsome, "A Comparison of Numerical Flux Formulas for the Euler and Navier-Stokes Equations," AIAA Paper No. 87-1104-CP, (June 1987).

14. Whitfield, D. L. and L. K. Taylor, "Discretized Newton-Relaxation Solution of High Resolution Flux-Difference Split Schemes," AIAA Paper No. 91-1539, (June 1991).

15. Baldwin, B. S. and H. Lomax, "Thin Layer Approximation and Algebraic Model for Separated Turbulent Flows," AIAA Paper No. 78-257, (1978).

16. Telste, J. G., R. M. Coleman and J. J. Gorski, "DTNS3D Computer Code Simulation of Tip-Vortex Formation: RANS Code Validation," NSWCCD-TR-20–97/013, (Aug. 1997).

17. Spalding, D. B., "A Single Formula for the Law of the Wall," *J. of App. Mechs.*, pp. 455–457 (Sept. 1961).

18. Lewandowski, E. M.,"The Effects of Reynolds Number, Section Shape, and Turbulence Stimulation on the Lift of a Series of Model Control Surfaces," *Proc. of the 22nd American Towing Tank Conf.*, pp. 398–407, (1989).